Data-driven Convexification for Frequency Nadir Constraint of Unit Commitment

Yukang Shen, Wenchuan Wu, *Fellow*, *IEEE*, Bin Wang, Yue Yang, and Yi Lin

***Abstract*—The increasing penetration of the renewable energy sources brings new challenges to the frequency security of power systems. In order to guarantee the system frequency security, frequency constraints are incorporated into unit commitment (UC) models. Due to the non-convex form of the frequency nadir constraint which makes the frequency constrained UC (FCUC) intractable, this letter proposes a revised support vector machine (SVM) based system parameter separating plane method to convexify it. Based on this data-driven convexification method, we obtain a tractable FCUC model which is formulated as a mixed-integer quadratic programming (MIQP) problem. Case studies indicate that the proposed method can obtain less conservative solution than the existing methods with higher efficiency.**

***Index Terms*—Unit commitment, frequency constraint, support vector machine (SVM), data-driven convexification.**

I. Introduction

With the integration of massive renewable energy sources (RESs) into power system, system operators face new challenges to ensure frequency stability. Since RESs are mostly connected to power grid by power electronic interfaces, the power system inertia is gradually decreasing with the growing share of RESs, which will deteriorate the frequency response performance of the power system [1].

There are some works on characterizing the frequency deviation of power systems after a disturbance. In [2]-[7], the frequency deviation is derived based on the swing equation, on the premise that the governor response of units is approximated as a ramp model. However, the approximation approach ignores the differences between the governor response models of each unit, so the frequency deviation result may involve large errors. In [8], a low-order frequency response model is proposed, which can derive the formulation of frequency deviation with the assumption that the generation is dominated by reheating steam turbine generators. In [9], the high-order frequency response model of the multi-machine system is directly solved, but the time-domain expression is too complicated. Reference [10] presents a method to aggregate the frequency response model of multi-machine system into a single-machine model.

In terms of frequency constrained unit commitment (FCUC) models, some efforts have been presented so far. The frequency constraints are derived in [11] based on the frequency response model of multi-machine system, and piece-wise linearization (PWL) technique is employed to linearize the nonlinear frequency nadir constraint (FNC), facilitating its integration in UC problem. The concept of frequency security margin is proposed to quantify the system frequency regulation ability in [12], and PWL technique is adopted to linearize it. However, the constraints containing piece-wise functions will cause high computational burden. In [13], a new linearization method for the nonlinear FNC is proposed, which recasts the nadir constraint by extracting bounds (EBs) on relevant variables of UC model. However, this linearization method may be very conservative. In [14] and [15], data-driven methods are used to reformulate the frequency constraints, such as classification decision tree and deep neural network, but these machine learning based methods may involve ultra-heavy computational burden since extra integer variables are introduced.

This letter proposes a revised support vector machine (SVM) based system parameter separating plane method to convexify the FNC. Based on this data-driven convexification method, we obtain a tractable FCUC model which is formulated as a mixed-integer quadratic programming (MIQP) problem. Finally, case studies indicate that our proposed method can obtain less conservative solution than the existing methods with higher efficiency.

II. Preliminaries

The frequency of power systems is closely linked with the real-time balance of active power. Figure 1 shows the frequency response model of the multi-machine system [11]. In Fig. 1, H is the total system inertia provided by conventional generators and RES; D is the load damping factor; R_i is the droop coefficient; K_{mi} is the mechanical power gain factor; F_{Hi} is the fraction of power generated by turbines; T_{Ri} is the turbine time constant; the subscript $i\,(i=1,2,\ldots,M)$ is the index of thermal generators; and ΔP_m and ΔP_e are the variations of mechanical power and electrical power, respec-

Manuscript received: November 2, 2021; revised: March 21, 2022; accepted: June 24, 2022. Date of CrossCheck: June 24, 2022. Date of online publication: July 15, 2022.

This work was supported in part by the S&T Project of State Grid Corporation of China "Learning based Renewable Cluster Control and Coordinated Dispatch" (No. 5100-202199512A-0-5-ZN).

Y. Shen, W. Wu (corresponding author), B. Wang, and Y. Yang are with the State Key Laboratory of Power Systems (Department of Electrical Engineering), Tsinghua University, Beijing 100084, China (e-mail: syk21@mails.tsinghua.edu.cn; wuwench@tsinghua.edu.cn; wb1984@tsinghua.edu.cn; yangyuethu@foxmail.com).

Y. Lin is with Electric Power Research Institute, Fujian Electric Power Ltd. Company, Fuzhou 350003, China (e-mail: jyy.lin_yi@fj.sgcc.com.cn).

DOI: 10.35833/MPCE.2021.000734

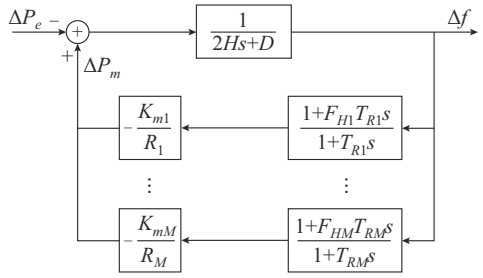

Fig. 1. Frequency response model of multi-machine system.

tively.

An analytical expression of the frequency dynamics $\Delta f(t)$ after a step disturbance ΔP can be derived as follows, under the assumption that $T_{Ri}=T(i=1,2,\ldots,M)$, and the detailed derivation can be found in [11].

$$\Delta f(t)=-\frac{\Delta P}{2HT\omega_n^2}-\frac{\Delta P}{2H\omega_r}\mathrm{e}^{-\zeta\omega_n t}\left(\sin(\omega_r t)-\frac{1}{\omega_n T}\sin(\omega_r t+\varphi)\right) \tag{1}$$

$$\begin{cases} F=\sum_{i=1}^{M}\dfrac{K_{mi}}{R_i}F_{Hi} \\ R=\sum_{i=1}^{M}\dfrac{K_{mi}}{R_i} \end{cases} \tag{2}$$

$$\begin{cases} \omega_n=\sqrt{\dfrac{D+R}{2HT}} \\ \zeta=\dfrac{2H+(D+F)T}{2\sqrt{2HT(D+R)}} \end{cases} \tag{3}$$

$$\begin{cases} \omega_r=\omega_n\sqrt{1-\zeta^2} \\ \varphi=\arcsin(\sqrt{1-\zeta^2}) \end{cases} \tag{4}$$

We concern about two frequency dynamic metrics, i. e., frequency nadir and rate of change of frequency (RoCoF), as shown in Fig. 2.

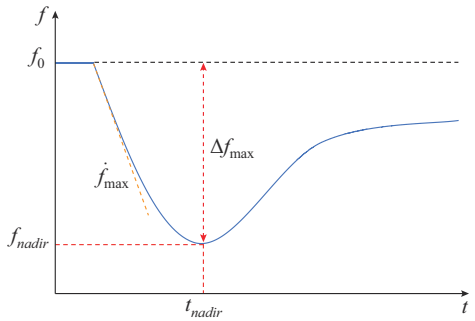

Fig. 2. Frequency dynamics after power disturbance.

For these two metrics, they should be kept within safe range after disturbance; otherwise, it may lead to frequency security violation. Then, the following frequency constraints should be satisfied:

$$t_{nadir}=\frac{1}{\omega_r}\arctan\left(\frac{\omega_r}{\zeta\omega_n-1/T}\right) \tag{5}$$

$$\Delta f_{\max}=\frac{f_0\Delta P}{R+D}\left(1+\mathrm{e}^{-\zeta\omega_n t_{nadir}}\sqrt{\frac{T(R-F)}{2H}}\right)\le\Delta f_{lim} \tag{6}$$

$$\dot{f}_{\max}=\frac{f_0\Delta P}{2H}\le\dot{f}_{lim} \tag{7}$$

where t_{nadir} is the time when the frequency reaches its nadir, i. e., f_{nadir}; f_0 is the base frequency; $\Delta f_{\max}$ and Δf_{lim} are the maximum frequency deviation and its threshold, respectively; and $\dot{f}_{\max}$ and $\dot{f}_{lim}$ are the maximum RoCoF and its threshold, respectively.

The power disturbance ΔP can be obtained by statistical analysis on historical data, and in this letter, we consider ΔP as a fixed value. Assuming that D and T are constant [11], the frequency constraints (6) and (7) are directly dependent on the system parameters H, R, and F. These system parameters can be linearly expressed as the decision variables in UC models. Unlike the linear RoCoF constraint (7), the FNC (6) is non-convex, which will make the FCUC intractable. Therefore, convexifying or linearizing constraint (6) is needed.

References [11] and [12] propose the PWL technique for obtaining the linearized FNC, facilitating its integration in UC problem. However, the constraint containing piece-wise functions also cause high computational burden. In [13], a new linearization method is proposed, which recasts the nadir constraint by extracting relaxed bounds on relevant variables of UC models as:

$$\begin{cases} H\ge H_{lim} \\ R\ge R_{lim} \\ F\ge F_{lim} \end{cases} \tag{8}$$

However, this linearization method in [13] is not suitable for large-scale power systems. For example, when the number of generators $M>40$, there will be more than 10^{12} generator commitment combinations. It is impossible to calculate all of these combinations. To avoid the high computational burden, we use Monte Carlo method to generate enough generator commitment combinations, e. g., 50000, for extracting bounds on relevant variables.

In addition, it is too conservative to directly convert the constraint (6) into (8). For example, when a system parameter, e.g., R, is appropriately less than its bound, and other parameters are appropriately larger than their bounds, the maximum frequency deviation may still be within the safe range, but this situation is outside the feasible set because it does not satisfy the constraint (8). That is to say, many "safe samples" would be misclassified due to the simple classification method.

In [14], the classification decision tree method is used to extract the frequency security constraints. Each leaf in the decision trees is labeled according to the dominant class of samples in population. It would be likely that some "unsafe samples" are included in a leaf flagged with safe label. The UC results from the decision tree method may violate constraint (6) because the decision tree method is under-conservative. The deep neutral network approach is employed to predict the frequency response in [15]. The frequency constraints are reformulated as a set of mixed-integer linear constraints, and the number of introduced integer variables is re-

lated to the scale of the neutral networks.

In summary, both the PWL technique and neutral networks approach will introduce extra integer variables in UC models, which lead to ultra-heavy computational burden. The convexification method in [13] is concise but over-conservative, while the decision tree method in [14] is under-conservative. Therefore, the convexification method for FNC in (6) needs to be improved.

III. Methodology

A. Linearization Method for FNC

Take the modified IEEE 24-bus system as an example. First, we generate data samples of the unit commitment by Monte Carlo method, and the scatter plot reflects the value of system parameters in 3-dimensional space, as presented in Fig. 3. The yellow points correspond to the unit combinations which satisfy the constraint (6), while the blue points correspond to those that do not satisfy. Enumerating all unit combinations is difficult and not worthwhile (30 generators correspond to more than 10^9 unit combinations), so in this example, we choose the sizes of training and test samples as 50000 and 5000, respectively. The size of training sample is proper because the training process is not time-consuming (around 1 s) and the results are accurate, as shown in Section IV.

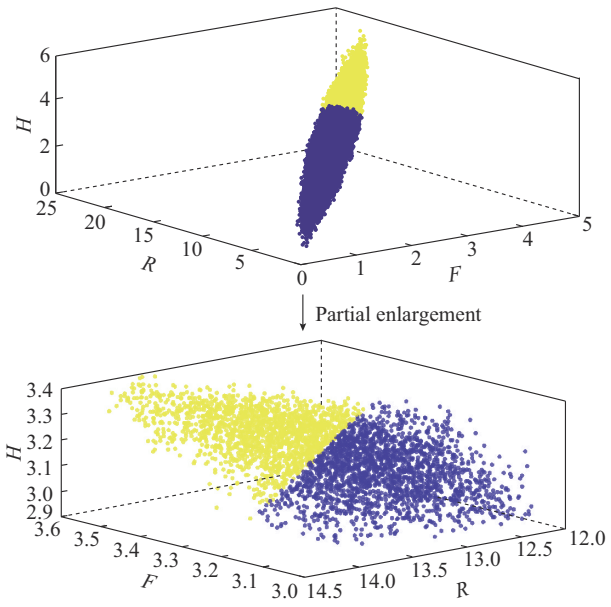

Fig. 3. System parameter scatter plot.

It is obvious that the blue points and the yellow points can be separated. If they can be linearly separated, the nonconvex constraint (6) could be converted into a linear one where the system parameter point is located above the separating plane. For deriving the separating plane, we can use the tool of SVM.

SVM is a classification learning method which can find a proper separating hyperplane based on training samples and separate samples into different categories. Figure 4 shows that there are many separating hyperplanes (dotted lines) that can separate samples, but only one (solid line) has the best effect. The optimal hyperplane maximizes the sum of the distances from the nearest two points to the separating hyperplane $\gamma = 2/\|\boldsymbol{\omega}\|$. The detailed solution of the SVM model can be found in [16].

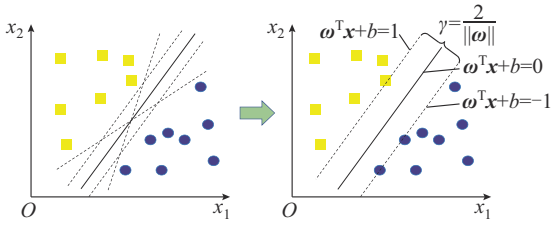

Fig. 4. SVM model.

It should be noted that the standard SVM model is derived based on the assumption that the data set can be linearly separated. If the training sample cannot be linearly separated, as shown in Fig. 5, the SVM model needs to be revised.

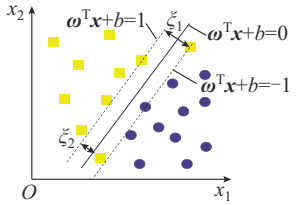

Fig. 5. Single soft margin SVM model for data set that cannot be linearly separated.

As shown in Fig. 5, by adding slack variable ξ, we can obtain a single soft margin SVM model. For system parameter points that do not satisfy the constraint (6) (blue points), we do not add slack variable ξ, while for points that satisfy the constraint (6) (yellow points), we add slack variable ξ, which means only the "safe samples" may be misclassified while the "unsafe samples" are kept correct. This classification model is conservative but reliable, which is formulated as:

$$\begin{cases} \min\limits_{\boldsymbol{\omega},b,\xi_i} \left\{ \dfrac{1}{2}\|\boldsymbol{\omega}\|^2 + C\sum\limits_{i=1}^{m}\xi_i \right\} \\ \text{s.t. } y_i(\boldsymbol{\omega}^{\mathrm{T}}\boldsymbol{x}_i + b) \geq 1-\xi_i \quad y_i = 1 \\ \qquad y_j(\boldsymbol{\omega}^{\mathrm{T}}\boldsymbol{x}_j + b) \geq 1 \quad y_j = -1 \\ \qquad \xi_i \geq 0 \quad i = 1,2,\ldots,m \end{cases} \tag{9}$$

where $\boldsymbol{\omega}$ is the normal vector of the hyperplane; b is the offset of the hyperplane from the origin; y is the label of data points, $y_i = 1$ for data points satisfies the constraint (6), while $y_j = -1$ for those do not satisfy; ξ_i is the slack variable; and C is the regularization parameter, which represents the penalty on the classification error.

Adding slack variable ξ only on the points that satisfy constraint (6) can ensure that all of other points that do not satisfy (6) are located on one side of the solved separating hyperplane for the reason that they have "hard margin". A conservative linear constraint will be obtained because some "safe samples" are misclassified, while this constraint could ensure all of the points above the hyperplane do not violate frequency security.

Figure 6 shows the system parameter scatter plot and its separating plane calculated by the single soft margin SVM model, for the same system as in Fig. 3. The points which are marked by black circles are the support vectors of the SVM model. Therefore, the non-convex constraint (6) can be convexified into the linear constraint (10), which represents the predicted safe class of the SVM model.

$$\omega_F F+\omega_R R+\omega_H H+b\geq 0 \tag{10}$$

where $\boldsymbol{\omega}=[\omega_F \quad \omega_R \quad \omega_H]^{\mathrm{T}}$ is the normal vector of the plane; and b is the offset of the plane from the origin.

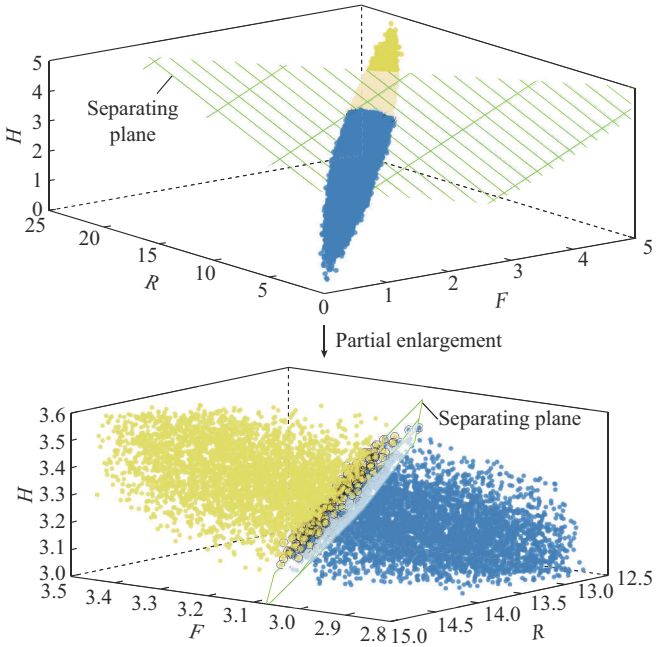

Fig. 6. System parameter scatter plot and its separating plane.

The constraint (10) is conservative to some extent. However, it is less conservative compared with the simple classification method proposed in [13] since the proposed method incurs less misclassified samples. In addition, the linearized constraint will not include extra integer variables.

Remark 1: load damping D also has a significant impact on frequency nadir. In practice, if D changes, (9) should be retrained to obtain hyperplanes corresponding to different values of D. Different hyperplanes can be added to UC model during different time periods. In this letter, we assume $T_{Ri}=T$ for all generators, and the impact of heterogeneous T_{Ri} on frequency nadir will be studied in our future work.

B. FCUC Model

By integrating the frequency constraints into traditional UC model, we can obtain a novel FCUC model. The objective function (11) is to minimize the total costs, which contain UC costs function (12) (start-up cost and shut-down cost), fuel costs function (13) (quadratic function on power output), wind power curtailment penalty function (14), and are subjected to power balance constraint (15), thermal generator constraints (16)-(18), the minimum up/down time constraints (19) - (22), wind power constraints (23) and (24), transmission line constraints (25) and (26), FNCs in (27) and (28), RoCoF constraint (29), and primary frequency regulation reserve constraint for thermal generators (30).

$$\min\left\{\sum_{t=1}^{T}\left[\sum_{i=1}^{M}(UC_i^t+FC_i^t)+\sum_{j=1}^{N}CP_j^t\right]\right\} \tag{11}$$

$$UC_i^t=\max\{SU_i\cdot(u_i^t-u_i^{t-1}),0\}+\max\{SD_i\cdot(u_i^{t-1}-u_i^t),0\} \tag{12}$$

$$FC_i^t=a_i(P_i^t)^2+b_iP_i^t+c_iu_i^t \tag{13}$$

$$CP_j^t=k_{j,cur}(W_{j,cur}^t)^2 \tag{14}$$

$$\sum_{i=1}^{M}P_i^t+\sum_{j=1}^{N}W_{j,sche}^t=\sum_{k=1}^{D}D_k^t \tag{15}$$

$$u_i^tP_{i,\min}\leq P_i^t\leq u_i^tP_{i,\max} \tag{16}$$

$$P_i^t-P_i^{t-1}\leq RU_i+(2-u_i^{t-1}-u_i^t)P_{i,\max} \tag{17}$$

$$P_i^{t-1}-P_i^t\leq RD_i+(2-u_i^{t-1}-u_i^t)P_{i,\max} \tag{18}$$

$$\sum_{m=t}^{t+UT_i-1}u_i^m\geq UT_i\cdot(u_i^t-u_i^{t-1})\quad\forall t=1,2,\ldots,T-UT_i+1 \tag{19}$$

$$\sum_{m=t}^{T}[u_i^m-(u_i^t-u_i^{t-1})]\geq 0\quad\forall t=T-UT_i+2,T-UT_i+3,\ldots,T \tag{20}$$

$$\sum_{m=t}^{t+DT_i-1}(1-u_i^m)\geq DT_i\cdot(u_i^{t-1}-u_i^t)\quad\forall t=1,2,\ldots,T-DT_i+1 \tag{21}$$

$$\sum_{m=t}^{T}[1-u_i^m-(u_i^{t-1}-u_i^t)]\geq 0\quad\forall t=T-DT_i+2,T-UT_i+3,\ldots,T \tag{22}$$

$$W_{j,sche}^t=W_{j,fore}^t-W_{j,cur}^t \tag{23}$$

$$0\leq W_{j,cur}^t\leq W_{j,fore}^t \tag{24}$$

$$\sum_{i=1}^{M}s_i^LP_i^t+\sum_{j=1}^{N}s_j^LW_{j,sche}^t-\sum_{k=1}^{D}s_k^LD_k^t\leq P_{\max}^L \tag{25}$$

$$\sum_{i=1}^{M}s_i^LP_i^t+\sum_{j=1}^{N}s_j^LW_{j,sche}^t-\sum_{k=1}^{D}s_k^LD_k^t\geq -P_{\max}^L \tag{26}$$

$$\omega_FF_{sys}^t+\omega_RR_{sys}^t+\omega_HH_{sys}^t+b\geq 0 \tag{27}$$

$$\begin{cases}R_{sys}^t=\dfrac{\sum_{i=1}^{M}u_i^t\frac{K_{mi}}{R_i}P_{i,\max}}{\sum_{i=1}^{M}P_{i,\max}+\sum_{j=1}^{N}P_{j,cap}}\\ H_{sys}^t=\dfrac{\sum_{i=1}^{M}u_i^tH_iP_{i,\max}+\sum_{j=1}^{N}H_jP_{j,cap}}{\sum_{i=1}^{M}P_{i,\max}+\sum_{j=1}^{N}P_{j,cap}}\\ F_{sys}^t=\dfrac{\sum_{i=1}^{M}u_i^t\frac{K_{mi}}{R_i}F_{Hi}P_{i,\max}}{\sum_{i=1}^{M}P_{i,\max}+\sum_{j=1}^{N}P_{j,cap}}\end{cases} \tag{28}$$

$$H_{sys}^t\geq\frac{f_0\Delta P}{2\dot{f}_{lim}} \tag{29}$$

$$P_{i,\max} - P_i^t \geq u_i^t \frac{K_{mi}}{R_i} P_{i,\max} \gamma \frac{\Delta f_{lim}}{f_0} \tag{30}$$

where t, i, j, and k are the indices of time, thermal generators, wind farms, and loads, respectively. For generator i, u_i^t and P_i^t are commitment status and power output, respectively; $P_{i,\max}$, $P_{i,\min}$, RU_i, and RD_i are the upper/lower power bounds and the upward/downward ramping limits, respectively; UT_i and DT_i are minimum up/down time, respectively; R_i, H_i, K_{mi}, and F_{Hi} are the frequency regulation parameters; UC_i^t is the UC cost depending on the adjacent commitment state; SU_i and SD_i are the cost coefficients of start-up and shut-down, respectively; FC_i^t is the fuel cost described with a quadratic function of power output; a_i, b_i, and c_i are the coefficients of the fuel cost function. For wind farm j, $W_{j,sche}^t$, $W_{j,cur}^t$, and $W_{j,fore}^t$ are the scheduled, curtailed, and forecasted wind power, respectively; $P_{j,cap}$ is the power capacity; H_j is the virtual inertia; CP_j^t is the curtailment penalty proportional to square of the curtailed wind power; $k_{j,cur}$ is the penalization coefficient; D_k^t is the power demand of load k; $P_{\max}^L$ is the power capacity of transmission line; s_i^L, s_j^L, and s_k^L are the power transfer distribution factors of generator i, wind farm j, and load k, respectively, and they are calculated by DC power flow model; F_{sys}^t, R_{sys}^t, and H_{sys}^t are the system parameters, which can be linearly expressed as the status variable u_i^t, and the total system capacity is set as the base value of power; and γ is the ratio of the steady-state value to the maximum value of frequency deviation, which is set to be 0.5 [12]. Constraint (30) ensures all of the online thermal generators have enough power reserve to deal with the power disturbance.

In summary, the formulations in (11) - (30) compose the proposed FCUC model which is formulated as an MIQP problem and can be efficiently solved by off-the-shelf solvers.

IV. Case Studies

The FCUC model is tested and compared with the existing model from [13] with a time resolution of 1 hour on modified IEEE 24-bus and 118-bus systems. The models are implemented in C++ and solved by CPLEX on a laptop with an Intel Core i7-10875H CPU and 16 GB RAM. For each test system, simulation results for three different UC models are reported: ① Model 1: without frequency constraints (11)-(26); ② Model 2: with frequency constraints from [13]; and ③ Model 3: with frequency constraints (11) - (30) proposed in this letter.

The difference between Model 2 and Model 3 is the formulation of FNC, where the former is (8) and the latter is (27). The linearization process for FNC of Models 2 and 3 are both solved in MATLAB R2021b. The power disturbance ΔP is set to be 250 MW and 650 MW for IEEE 24-bus and 118-bus systems, respectively. They are both almost equivalent to the capacity of the biggest generator of each test system. The base frequency is 50 Hz, the frequency nadir threshold is 49.5 Hz, and the maximum allowable RoCoF is 0.5 Hz/s. Table I shows the frequency regulation parameters of thermal generators and wind farms for the two test systems.

TABLE I
Frequency Regulation Parameters of Thermal Generators and Wind Farms

Type	H (s)	K_m/R (p.u.)	F_H (p.u.)
Thermal generator	4.0-7.5	15-30	0.15-0.30
Wind farm	3.0-5.0		

The linearization processes for FNC of Model 2 (EB) and Model 3 (SVM) are two different classification models. We first perform evaluation on these two classification models with two evaluation indices: *Precision* and *Recall*. For a binary classification model, all data samples can be classified into one of the four groups: true positive (TP), false positive (FP), false negative (FN), and true negative (TN), as shown in Fig. 7.

		True condition	
		1	-1
Predicted condition	1	TP	F P
	-1	FN	TN

Fig. 7. Four groups of binary classification.

The evaluation indices *Precision* and *Recall* can be calculated as:

$$Precision = \frac{num(TP)}{num(TP) + num(FP)} \tag{31}$$

$$Recall = \frac{num(TP)}{num(TP) + num(FN)} \tag{32}$$

where $num(\cdot)$ is the number of the samples which belong to the corresponding group.

Precision reflects the reliability of the classification model, while *Recall* reflects its conservatism. The lower *Recall*, the more "safe samples" are predicted as "unsafe samples". Tables II and III show the evaluation indices on the two classification models in IEEE 24-bus and 118-bus systems, respectively.

TABLE II
Evaluation Indices of Two Classification Models in IEEE 24-bus System

Model	Sample	*Precision* (%)	*Recall* (%)
Model 2 (EB)	Training sample	100	79.29
	Test sample	100	79.76
Model 3 (SVM)	Training sample	100	98.25
	Test sample	100	98.21

TABLE III
Evaluation Indices of Two Classification Models in IEEE 118-bus System

Model	Sample	*Precision* (%)	*Recall* (%)
Model 2 (EB)	Training sample	100	76.85
	Test sample	100	75.77
Model 3 (SVM)	Training sample	100	95.86
	Test sample	100	96.50

The results show that *Precision* of the two classification models are both 100%, so that the classification rules are both reliable on the training sample and test sample. However, *Recall* of Model 2 (EB) is much lower than that of Model 3 (SVM), which means more "safe samples" of Model 2 (EB) are predicted incorrectly. As a result, the constraint (8) in Model 2 is much more conservative than (27) in Model 3, and it would cause extra cost in operation.

Remark 2: the disadvantage of both the method in [13] and the proposed method is that the results are conservative. However, to stabilize the frequency for power systems under disturbance, such conservativeness is acceptable. The results in Tables II and III show that our proposed method reduces the conservativeness compared with the method in [13]. In practice, *Precision* and *Recall* should be calculated after SVM training to evaluate the conservativeness. Based on the two evaluation indices, system operators can judge whether the convex constraint (10) is applicable to the specific power grid.

The results of the three UC models tested on IEEE 24-bus and 118-bus systems are summarized in Tables IV and V, where the mixed-integer programming gaps are 0.1% and 1%, respectively. The operation cost (objective function minus wind curtailment penalty) represents the total cost for thermal generators. The linearizing FNC time (LFT) includes both the time for generating data sample and the time for training classification model. Owing to incorporating linear frequency constraint, the proposed FCUC model can be solved efficiently. Table IV shows that the solution time of FCUC models is less than that of Model 1, since the added linear constraints reduce the solution space.

TABLE IV
COMPARISON OF RESULTS OF THREE MODELS IN IEEE 24-BUS SYSTEM

Model	Objective function ($)	Operation cost ($)	Wind curtailment (%)	Frequency violation	LFT (s)	Solution time for UC (s)
Model 1	733838	355355	7.82	Yes		3.11
Model 2	847840	443987	8.08	No	0.91	1.88
Model 3	839173	440394	7.90	No	1.06	1.55

TABLE V
COMPARISON OF RESULTS OF THREE MODELS IN IEEE 118-BUS SYSTEM

Model	Objective function ($)	Operation cost ($)	Wind curtailment (%)	Frequency violation	LFT (s)	Solution time for UC (s)
Model 1	2979295	2979295	0	Yes		25.45
Model 2	3009581	3006376	0.27	No	0.92	94.14
Model 3	3000776	3000408	0.09	No	1.04	51.20

We use the system frequency response model to compare the frequency dynamics of the three UC models after the disturbances on IEEE 24-bus and 118-bus systems, as shown in Figs. 8 and 9, respectively. In order to eliminate frequency violations, more thermal generators need to be scheduled online, which will increase the operation cost and wind curtailment. Compared with Model 2, the frequency nadir of Model 3 is much closer to the threshold for the reason that the constraint (27) is less conservative than (8). For Model 3, fewer thermal generators need to be scheduled online than Model 2. Therefore, the operation cost and wind curtailment of Model 3 are both lower than those of Model 2, which indicates that our proposed FCUC model is more effective.

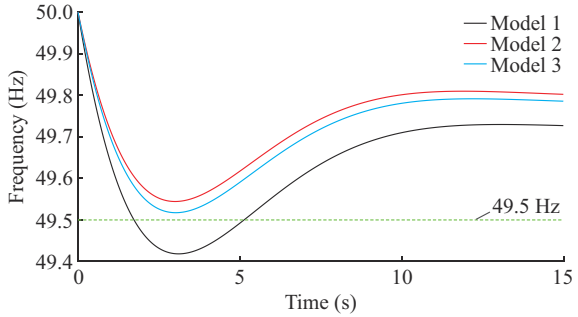

Fig. 8. Frequency dynamics after disturbance on IEEE 24-bus system at the 12th hour.

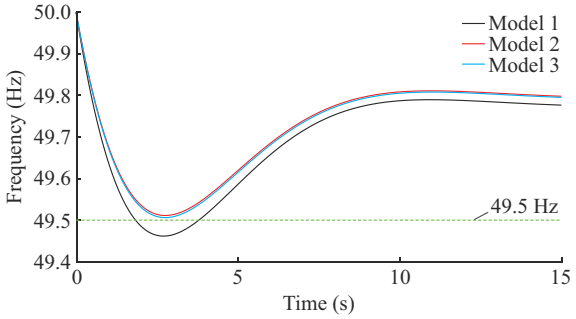

Fig. 9. Frequency dynamics after disturbance on IEEE 118-bus system at the 24th hour.

V. CONCLUSION

This letter proposes a revised SVM-based system parameter separating plane method to convexify the non-convex FNC. Based on this data-driven converification method, we obtain a novel FCUC model which can be formulated as a tractable MIQP problem. Case studies indicate that the proposed method can obtain much less conservative solution than the existing methods with high efficiency.

REFERENCES

[1] A. Ulbig, T. S. Borsche, and G. Andersson, "Impact of low rotational inertia on power system stability and operation," *IFAC Proceedings*

Volumes, vol. 47, pp. 7290-7297, Aug. 2014.
[2] H. Chávez, R. Baldick, and S. Sharma, "Governor rate-constrained OPF for primary frequency control adequacy," *IEEE Transactions on Power Systems*, vol. 29, no. 3, pp. 1473-1480, May 2014.
[3] F. Teng, V. Trovato, and G. Strbac, "Stochastic scheduling with inertia-dependent fast frequency response requirements," *IEEE Transactions on Power Systems*, vol. 31, no. 2, pp. 1557-1566, Mar. 2016.
[4] G. Zhang, E. Ela, and Q. Wang, "Market scheduling and pricing for primary and secondary frequency reserve," *IEEE Transactions on Power Systems*, vol. 34, no. 4, pp. 2914-2924, Jul. 2019.
[5] L. Badesa, F. Teng, and G. Strbac, "Simultaneous scheduling of multiple frequency services in stochastic unit commitment," *IEEE Transactions on Power Systems*, vol. 34, no. 5, pp. 3858-3868, Sept. 2019.
[6] L. Badesa, F. Teng, and G. Strbac, "Optimal portfolio of distinct frequency response services in low-inertia systems," *IEEE Transactions on Power Systems*, vol. 35, no. 6, pp. 4459-4469, Nov. 2020.
[7] Z. Chu, U. Markovic, G. Hug *et al*., "Towards optimal system scheduling with synthetic inertia provision from wind turbines," *IEEE Transactions on Power Systems*, vol. 35, no. 5, pp. 4056-4066, Sept. 2020.
[8] P. M. Anderson and M. Mirheydar, "A low-order system frequency response model," *IEEE Transactions on Power Systems*, vol. 5, no. 3, pp. 720-729, Aug. 1990.
[9] D. L. H. Aik, "A general-order system frequency response model incorporating load shedding: analytic modeling and applications," *IEEE Transactions on Power Systems*, vol. 21, no. 2, pp. 709-717, May 2006.
[10] Q. Shi, F. Li, and H. Cui, "Analytical method to aggregate multi-machine SFR model with applications in power system dynamic studies," *IEEE Transactions on Power Systems*, vol. 33, no. 6, pp. 6355-6367, Nov. 2018.
[11] H. Ahmadi and H. Ghasemi, "Security-constrained unit commitment with linearized system frequency limit constraints," *IEEE Transactions on Power Systems*, vol. 29, no. 4, pp. 1536-1545, Jul. 2014.
[12] Z. Zhang, E. Du, F. Teng *et al*., "Modeling frequency dynamics in unit commitment with a high share of renewable energy," *IEEE Transactions on Power Systems*, vol. 35, no. 6, pp. 4383-4395, Nov. 2020.
[13] M. Paturet, U. Markovic, S. Delikaraoglou *et al*., "Stochastic unit commitment in low-inertia grids," *IEEE Transactions on Power Systems*, vol. 35, no. 5, pp. 3448-3458, Sept. 2020.
[14] D. T. Lagos and N. D. Hatziargyriou, "Data-driven frequency dynamic unit commitment for island systems with high RES penetration," *IEEE Transactions on Power Systems*, vol. 36, no. 5, pp. 4699-4711, Sept. 2021.
[15] Y. Zhang, H. Cui, J. Liu *et al*., "Encoding frequency constraints in preventive unit commitment using deep learning with region-of-interest active sampling," *IEEE Transactions on Power Systems*, vol. 37, no. 3, pp. 1942-1955, May 2022.
[16] M. O. Stitson, J. A. E. Weston, A. Gammerman *et al*., "Theory of support vector machines," University of London, Tech. CSD-TR-96-17, Dec. 1996: 188-191.

Yukang Shen received the B. S. degree from Xi'an Jiaotong University Xi'an, China, in 2021. He is currently working toward the Ph. D. degree with the Department of Electrical Engineering, Tsinghua University, Beijing, China. His research interests include optimization and control in power system considering frequency stability.

Wenchuan Wu received the B.S., M.S., and Ph.D. degrees from the Electrical Engineering Department, Tsinghua University, Beijing, China. He is currently a Professor with Tsinghua University, Deputy Director of the State Key Laboratory of Power Systems, Tsinghua University, and IEEE Fellow. He was a recipient of the National Science Fund of China Distinguished Young Scholar Award in 2017. His research interests include energy management system, active distribution system operation and control, machine learning and its application in energy system.

Bin Wang received the B. S. and Ph. D. degrees in electrical engineering from Tsinghua University, Beijing, China, in 2005 and 2011, respectively. He is currently an Associate Professor with the Department of Electrical Engineering, Tsinghua University. His research interests include renewable energy optimal dispatch and control, and automatic voltage control.

Yue Yang received the B.S. degree from the Electrical Engineering Department, Tsinghua University, Beijing, China, in 2017. He joined the State Key Laboratory of Power Systems, Tsinghua University, in September 2017, where he is currently working toward the Ph.D. degree. His research interests include optimization and control in power system with integration of renewable generation.

Yi Lin is an Engineer with Electric Power Research Institute, Fujian Electric Power Ltd. Company, Fuzhou, China. His research interests include distribution network planning and operation.